Ecological Indicators 96 (2019) 669–683

Contents lists available at ScienceDirect

Ecological Indicators

journal homepage: www.elsevier.com/locate/ecolind

Spatiotemporal variations of extreme climate events in Northeast China during 1960–2014

Enliang Guo[a,b,c], Jiquan Zhang[d,*], Yongfang Wang[e], Lai Quan[a,b,c], Rongju Zhang[f], Feng Zhang[d], Mo Zhou[d]

[a] College of Geographical Science, Inner Mongolia Normal University, Hohhot 010022, PR China
[b] Inner Mongolia Key Laboratory of Disaster and Ecological Security on the Mongolian Plateau, Inner Mongolia Normal University, Hohhot 010022, PR China
[c] Inner Mongolia Key Laboratory of Remote Sensing and Geographic Information Systems, Inner Mongolia Normal University, Hohhot 010022, PR China
[d] School of Environment, Northeast Normal University, Changchun 130024, PR China
[e] Grassland Research Institute, Chinese Academy of Agricultural Science, Hohhot 010022, PR China
[f] Ewenki Autonomous Banner Meteorological Bureau, HulunBuir 021100, PR China

ARTICLE INFO

Keywords:
Extreme climate indices
Non-linear tendency
Periodic oscillation
Trivariate copula
Joint return periods

ABSTRACT

With the acceleration of global warming, the frequent occurrence of extreme climate events has inflicted great socio-economies losses and casualties; therefore, it is particularly important to explore the characteristics of extreme climate events. Nine extreme climate indices defined by the World Meteorological Organization's Expert Team on Climate Change Detection and Indices (ETCCDI) were constructed from a long term (1960–2014) continuous dataset of 70 meteorological stations in Northeast China (NEC). We detected the current and future spatial variation characteristics using the Sen's slope estimator and R/S analysis method, respectively, and periodicities of individual extreme climate indices were calculated by Morlet continuous wavelet transform methods. Furthermore, a variety of marginal distribution functions was adopted to construct trivariate copula functions in order to calculate the joint probabilities and return periods. The results show that there were different spatiotemporal variation patterns of extreme climate indices: the extreme cold temperature index frost days (FD0) had a significant decreasing trend, summer days (SU25), tropical nights (TR20), and warm days (TX90) had a significant increasing trend. However, no significant changes in the extreme precipitation indices were detected consistently; only a few stations scattered over NEC showed significant changes in these indices. Most of the extreme temperature indices showed significant periods of about 1.5, 2, and 3 years, whereas extreme cold and precipitation indices had approximate periods of 3, 3.5, and 4 years. Southeastern Jilin and northeastern Liaoning Provinces had colder winters and higher annual precipitation than other regions. The probabilities of high temperatures and heavy precipitation were relatively high in western Liaoning, Jilin, and Heilongjiang Provinces.

1. Introduction

Climate warming has led to significant changes in and challenges to water and heat resources and resource management worldwide. Extreme climate events, in particular, are sensitive to climate change and have become greater hazards to humans, socio-economies, and ecosystems (Zhou and Ren, 2011; Barlow et al., 2015; El-Zein and Tonmoy, 2015; Bahinipati and Venkatachalam, 2016; Qian et al., 2016; Zhang et al., 2016). Thus, it has been attracting wide attention since the 1990s, with a great deal of evidence indicating that the frequency and intensity of extreme climate events have increased (Zhang et al., 2013). Numerous extreme temperature events have been observed in regions worldwide, such as eastern United States, the Koshi river basin (Tibet, Nepal, and India), South Africa and Hokkaido, where it has been demonstrated that cold days, cold nights and frost days have become less frequent, whereas hot days, hot nights and heat waves have occurred more frequently in these locations (Mutiibwa et al., 2015; Shrestha et al., 2016; van Wilgen et al., 2016; Wang et al., 2016a,b). In addition, the temporal and spatial distributions of precipitation changes caused by increasing temperatures have led to increased frequency and intensity of extreme climate events, such as droughts and floods, and have exacerbated the effects of such extreme events (Kreft et al., 2014; Lesk et al., 2016; Wang et al., 2016a,b). Therefore, study of extreme climate events, especially multi-extreme climate events, is critically important.

* Corresponding author.
E-mail address: zhangjq022@nenu.edu.cn (J. Zhang).

https://doi.org/10.1016/j.ecolind.2018.09.034
Received 6 January 2017; Received in revised form 12 September 2018; Accepted 14 September 2018
Available online 09 October 2018
1470-160X/ © 2018 Elsevier Ltd. All rights reserved.

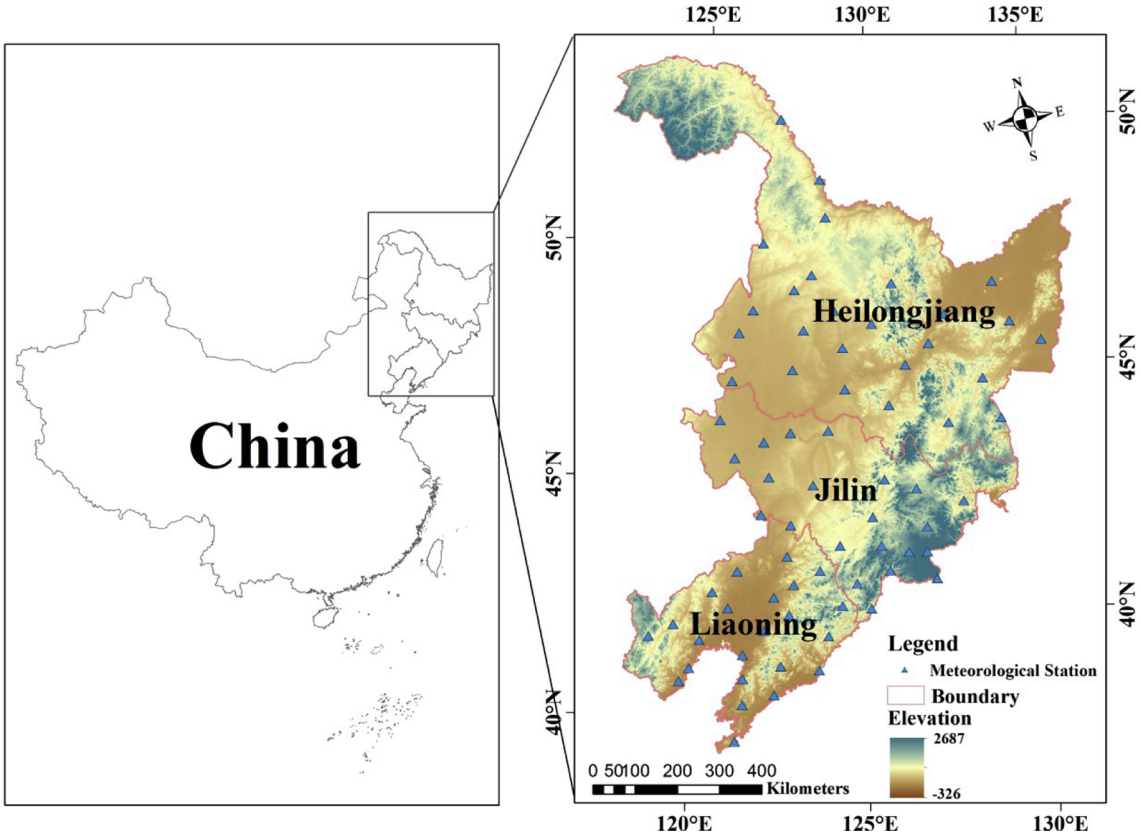

Fig. 1. Map of the study area.

The frequent occurrence of extreme climate events has inflicted major casualties and social and economic losses; therefore, many scholars have focused and intensified their research on such events (Farajzadeh et al., 2015; Keggenhoff et al., 2014; Ruml et al., 2017). The representation of extreme climate changes requires the use of certain indices. To eliminate the differences between the natural conditions of the various countries and the expression habits of the indices, the World Meteorological Organization's Expert Team on Climate Change Detection and Indices (ETCCDI) approved a list of 40 indices, 27 of which were considered core indices (Zhou and Ren 2011). At present, numerous scientists have investigated a series of studies about extreme climate events. The first of these components is determining extreme climate event thresholds (Hou et al., 2011). For example, Yang et al., (2008) determined the thresholds of extreme events using detrended fluctuation analysis. A default Bayesian method has also been adopted to determine extreme climate events (Cabras et al., 2011). The second component is evaluating the change trends of different kinds of extreme climate indices, which are focused mainly on the frequency, intensity, and trends of extreme temperature and precipitation events. For example, García-Cueto et al. (2014) analyzed and modelled extreme temperatures in northwestern Mexico and showed that extreme maximum summer temperature increases 4–5 °C and 2–3 °C under the low (RCP4.5) and high (RCP8.5) radiative forgings, respectively. Wang et al. (2017) investigated the spatiotemporal trends of temperature and precipitation extremes indicesfrom ETCCDI in the Loess Plateau region of China, and found widespread significant warming trends for all the temperature extremes except for the diurnal temperature range (DTR), and a larger percentage of areas show significant drying trends for precipitation indices generally over the southeast. The third component involves determining the attribution of extreme climate events. For example, Duan et al. (2015) detected possible correlations between climate indices and extreme precipitation events in Japan during the period 1901–2012. Gao and Shi (2016)analyzed the relationship between extreme precipitation events and large-scale atmospheric circulation. Although previous studies of extreme events have often focused on individual events, the probability distribution of multiple extreme events has also been analyzed based on individual probability distribution or bivariate copula joint probability (Zhang et al., 2011, 2013; Li et al., 2015). Nevertheless, there has been insufficient study of the probability characteristics of multiple extreme events occurring alternately or simultaneously, i.e., the joint probability characteristics of extreme temperature and extreme precipitation events have received relatively little attention. It is particularly important to assess the joint probabilistic characteristics and tendencies of trivariate extreme climate events in the context of global warming and increasingly frequent abrupt drought–flood alternation events.

The three provinces of Northeast China (NEC), i.e., Liaoning, Jilin, and Heilongjiang, have a temperate monsoon climate with great variation in precipitation. The annual mean temperature in NEC has increased by about 1.56 °C during 1961–2012 (Hu et al., 2016), which makes this one of the most sensitive regions to global warming in China for extreme temperature and precipitation events. There have been a number of studies on extreme weather events in NEC (Yu and Li, 2015; Du et al., 2013a,b). However, the previous studies in NEC have focused mainly on the spatiotemporal variation of individual extreme climate indices. Therefore, in this study, we have analyzed the joint distribution of trivariate extreme climate events, which is of great significance for prediction and early warning of abrupt dry–wet transitions and for water resource management, based on daily meteorological data (daily minimum, maximum, and mean temperatures, as well as daily precipitation) in NEC. The ensemble empirical mode decomposition (EEMD) method, Sen's slope method, R/S analysis method and Morlet continuous wavelet transform were adopted to analyze the spatiotemporal variation characteristics of nine individual extreme climate indices, and trivariate copula functions were applied to investigate the probabilistic characteristics of extreme climate events. The results will

help in understanding changes in extreme climate events in NEC and in exploring the causes of regional climate change. This study also provides a scientific basis for future prediction of extreme climate events and may contribute to natural disaster prevention and mitigation.

2. Study area

Northeast China (38°43′–53°33′N, 118°53′–135°05′E), which covers a total area of 7.91×10^5 km^2, was selected as the study area (Fig. 1). It is surrounded by mountains on three sides and bounded by the Bohai Sea to the south; the Sanjiang, Songnen, and Liaohe plains extend across the central region of NEC. The study area is a region with cold temperate to mid-temperate and humid to semi-humid climate (Zhao et al., 2012). Precipitation is unevenly distributed spatiotemporally over NEC, the annual amounts ranging from 450 to 1070 mm and with 60% recorded between July and September, which decrease substantially from southeast to northwest (Zhao et al., 2015). NEC is considered as one of the world's three largest “golden maize belts", which is a high maize production zone in China (Li et al., 2014; Lin et al., 2017). Because of the specific characteristics of this geographic location, the impacts of climate disasters on crop production in this region are particularly severe (Zhao et al., 2016).

3. Materials and methods

3.1. Materials

Daily weather data collected from 1960 to 2014 of 70 meteorological stations were downloaded from the China Meteorological Administration data network (http://data.cma.cn/); these data include daily precipitation and temperature data. 26 stations are located in Heilongjiang Province, 21 stations in Jilin Province, and 23stations in Liaoning Province. The nine extreme climate indices used in this study, as defined by RClimDexV3, are shown in Table 1.

3.2. Methods

3.2.1. Sen's slope estimator

If a linear trend is present in a time series, the true slope (change per unit time) can be estimated using Sen's slope estimator method, a simple non-parametric procedure developed by Sen (1968). Compared with the linear trend of least squares fitting, Sen's slope can avoid the missing data in a time series and eliminate the influence of outliers (Gocic and Trajkovic, 2013). The formula to calculate Sen's slope is:

$$Q_k = median\frac{(X_j - X_i)}{j-i}\ (\ k = 1,\ldots,N), \tag{1}$$

where X_j and X_i are data values at times j and i ($j > i$), respectively. The median of these N values of Q_k is Sen's slope. In this study, this method was adopted to detect trends in the spatial change of the extreme climate indices.

3.2.2. Morlet continuous wavelet transform

Wavelet analysis can be used to detect the position of each time in each cycle by using expand signal to a bivariate pattern, which can be used to better analyze changes in the time series (Goupillaud et al., 1984). In recent years, this method has been widely used to analyze the characteristics of climate and multi-scale hydrology (Sang, 2013; Wen et al., 2016; Agarwal et al., 2016a,b; Tamaddun et al., 2017). In this study, continuous transform with Morlet wavelet function was chosen, as it can discriminate the periodic size of the time series and the distribution of these periods in the time domain and provide the change in the amplitude and phase information of the time series (Nicolay et al., 2009; Narasimha and Bhattacharyya, 2010). The Morlet wavelet $\varphi(t)$ is defined as:

$$\psi_0(\eta) = \pi^{-1/4} e^{iw_0 t} e^{-\eta^2/2}, \tag{2}$$

where w_0 is the dimensionless frequency, 32 was chosen as the wavelet permissibility condition, η is a non-dimensional time parameter, and $i$is the unit of an imaginary number (Farge, 1992; Torrence and Compo, 1998). The continuous wavelet transform of a discrete signal $f(t)$ with a Morlet wavelet $\psi(t)$ is:

$$W_f(a, b) = \frac{1}{a}\int_R f(t)\psi^* \times \left(\frac{t-b}{a}\right)dt, \tag{3}$$

where $W_f(a, b)$ is the transform coefficient; a and b are the scale parameter and translation parameter, respectively; ψ^* is the complex conjugate; and t is the time scale (Zeng et al., 2016).

To test the significance of the cycle more accurately, the wavelet power spectrum, which is defined as $|W_n^X(s)|^2$, must be calculated. The wavelet power spectrum can be averaged over a certain period, and the global wavelet spectrum of the wavelet can thus be obtained as:

$$\overline{W}^2(s) = \frac{1}{N}\sum_{n=0}^{N-1} |W_n(s)|^2. \tag{4}$$

The global wavelet spectrum can show the unbiased and unanimous estimate of the real power spectrum of the time series (Torrence and Compo, 1998). In addition, edge effect and significance test of wavelet power spectrum can be referred to Torrence and Compo (1998).

3.2.3. Ensemble empirical mode decomposition

Ensemble empirical mode decomposition (EEMD) is a type of self-adaptive time-series analysis technique that was developed in recent years and is suitable for analysing non-linear and non-stationary time series. It is an improved version of empirical mode decomposition (Wu and Huang, 2009). The mixing mode of empirical mode decomposition was improved, and the decomposition results become more stable. The EEMD method is based on the principle of multiple averaged measurements, by adding an appropriate size white noise in the original observation data to simulate multiple scenarios, and the calculation is made after repeated ensemble mean (Qian et al., 2016).

Table 1
Extreme climate indices defined by RClimDexV3.

Indicator	Descriptive name	Definition	Unit
FD0	Frost days	Annual count when TN (daily minimum temperature) < 0 °C	Days
SU25	Summer days	Annual count when TX (daily maximum temperature) > 25 °C	Days
TR20	Tropical nights	Annual count when TN (daily minimum temperature) > 20 °C	Days
TX10p	Cool days	Percentage of days when TX < 10th percentile	Days
TX90p	Warm days	Percentage of days when TX > 90th percentile	Days
CDD	Consecutive dry days	Maximum number of consecutive days with RR < 1 mm	Days
CWD	Consecutive wet days	Maximum number of consecutive days with RR ≥ 1 mm	Days
R95pTOT	Very wet days	Annual total PRCP when RR > 95th percentile	mm
PRCPTOT	Annual total wet-day precipitation	Annual total PRCP on wet days (RR ≥ 1 mm)	mm

Note: PRCP is an abbreviation of precipitation, RR s an abbreviation of daily precipitation.

3.2.4. R/S analysis method

The R/S analysis method has developed into a fractal theory for studying time series, which has been widely used in the study of urban environmental change, climate change, population, and economic development (Graham et al., 2012; Peng et al., 2012). In the climate aspect, the R/S analysis method can be used to predict future climate trends, the main principle is to construct a time series$\{\xi(t), t = 1, 2....\}$, for any positive integer $\tau \geq 1$, define a mean sequence:

$$\langle\xi\rangle_\tau = \frac{1}{\tau}\sum_{t=1}^{\tau}\xi(t)\tau = 1, 2.... \tag{5}$$

Cumulative deviation:

$$X(t, \tau) = \sum_{\mu=1}^{t}(\xi(\mu)-\langle\xi\rangle_\tau)1 \leq t \geq \tau \tag{6}$$

The range:

$$R(\tau) = \max_{1\leq t\geq\tau} X(t, \tau)- \min_{1\leq t\geq\tau} X(t, \tau)\tau = 1, 2.... \tag{7}$$

Standard deviation:

$$S(\tau) = \left[\frac{1}{\tau}\sum_{t=1}^{\tau}(\xi(t)-\langle\xi\rangle_\tau)^2\right]^{\frac{1}{2}} \tag{8}$$

For $R(\tau)/S(\tau) \triangleq R/S$, If there is a relationship as follows:

$$R/S \propto \tau^H \tag{9}$$

Indicating that the time series exists Hurst phenomenon, H is called the Hurst index. According to the value of $(\tau, R/S)$, H can be obtained by least squares fitting formula (5) in a double logarithmic coordinate system. According to the H value, whether the sequence is completely random or there is a trend component can be determined, and the trend component is expressed as persistent or anti-persistent, with $H = 0.5$ indicating that climate change is random, $0.5 < H < 1$ that climate change is sustainable, and $0 < H < 0.5$ that future climate change is opposite to that of the past.

3.2.5. Trivariate copula functions

Copulas, initially proposed by Sklar (1959), can be linked to a number of variables with arbitrary marginal distribution and the joint distribution function, regardless of their original marginal distributions (Miao et al., 2016). Copula functions are helpful in understanding the critical behaviour of variables and can be used to derive the joint distribution of two or more variables (Ganguli and Reddy, 2013a; Chang et al., 2016). Currently, copula functions are widely used to establish probability in studies on floods, droughts, and other climate extremes, in which the copula functions have begun to shift from bivariate copula to trivariate copula functions (Ganguli and Reddy, 2013b; Zhang and Singh, 2014; Ma et al., 2013; Saghafian and Mehdikhani, 2014; Miao et al., 2016). To describe the accuracy characteristics of spatiotemporal variations of extreme climate indices in NEC, trivariate copula functions have been used to calculate the return periods of extreme climate indices. Commonly used trivariate Archimedean copula functions include the Frank, Gumbel, and Clayton copula functions; these distribution functions and their parameters are shown in Table 2.

In this study, the following steps were carried out to calculate the trivariate Archimedean copula functions. (i) Normal distribution (NORM), Poisson distribution (POISS), exponential distribution (EXP), extreme value distribution (EV), the generalized extreme value distribution (GEV), the generalized Pareto distribution (GP), and gamma distribution (GAMA) were adopted to determine the marginal distribution of each extreme climate index. Moreover, corresponding parameters were estimated, and the Kolmogorov–Smirnov goodness-of-fit test (K–S test) was then applied to evaluate the statistical performance of the distributions of each extreme climate index. (ii) Correlation was measured between the extreme climate indices using Kendell's rank correlation coefficients. (iii) The parameters of the copula functions were estimated. (iv) The copula function parameter fitting of the trivariate extreme climate indices was evaluated, and the optimal copula function was selected using the minimum principle of the AIC criterion and the root-mean-square error (RMSE). (v) Finally, the trivariate joint distribution model was constructed (Wang et al., 2015).

Table 2
Trivariate Archimedean copula functions.

Copula function	$C(u, v, w)$	Parameter range
Frank	$-\frac{1}{\theta}\ln\left[1+\frac{(e^{-\theta u}-1)(e^{-\theta v}-1)(e^{-\theta w}-1)}{(e^{-\theta}-1)^2}\right]$	$(-\infty, \infty)\backslash\{0\}$
Clayton	$max\left[(u^{-\theta}+v^{-\theta}+w^{-\theta}-2)^{-\frac{1}{\theta}}, 0\right]$	$[-1, \infty]\backslash\{0\}$
Gumbel	$exp\left\{-[(-\ln u)^\theta+(-\ln v)^\theta+(-\ln w)^\theta]^{\frac{1}{\theta}}\right\}$	$[1, \infty]$

The return period was calculated as the mean of the trivariate copula function:

$$T_\alpha = \frac{1}{P(D\cdot d\ UI\cdot iUS\cdot s)} = \frac{1}{1-C(u, v, w)} \tag{10}$$

where T_α is the trivariate joint return period; and D, S, and I denote extreme climate indices.

4. Results

4.1. Temporal variability analysis

Extreme climate indices averaged over 70 stations in NEC were calculated using the ensemble empirical mode decomposition (EEMD) method, of which trend component and inter-decadal variations are shown in Fig. 2. It can be seen that most of the extreme warm indices, including SU25, TR20, and TX90P, showed an increasing trend, whereas the extreme precipitation indices, including CWD, R95pTOT, and PRCPTOT, had decreasing trends. The results indicated that the climate of NEC tends toward warm and dry conditions. In addition, uptrends of CDD and downtrends of FD0 and TX10P also provide evidence for this finding. From the inter-decadal variations of the extreme climatic indices, it can be seen that the 1980s witnessed extreme precipitation events relatively frequently, with obvious wave peaks in CWD, R95pTOT, and PRCPTOT. However, in the 1990s, the extreme precipitation indices started to decrease, whereas SU25, TR20, TX90P, and the dryness index (CDD) showed upward trends. This indicates that extreme warm events were dominant in this period, when climate warming and drying trends were accelerating in NEC. Further analysis of the other indices demonstrated that they do not share the same rate of change, with the trend of FD0 close to linear and having the greatest amplitude among the indices and TX10P fluctuating throughout the study period.

4.2. Periodic oscillation analysis

The variations of extreme climate indices are complex and often expressed as multi-frequency and quasi-periodic vibrations in the time domain. Therefore, it is helpful to use Morlet wavelet transformation for extreme climate indices averaged over 70 stations in NEC during 1960–2014 for understanding the regularity of the climate period and for predicting the response to climate change. Fig. 3 shows the wavelet power spectrum of the extreme climatic indices, in which the larger the wavelet powers are, the more intensive the contours are. The influence cone indicates that the partial wavelet power spectrum is affected by the edge effect, and there is a large uncertainty in the periodic characteristics (Zhang et al., 2007). In addition, the global wavelet spectrum

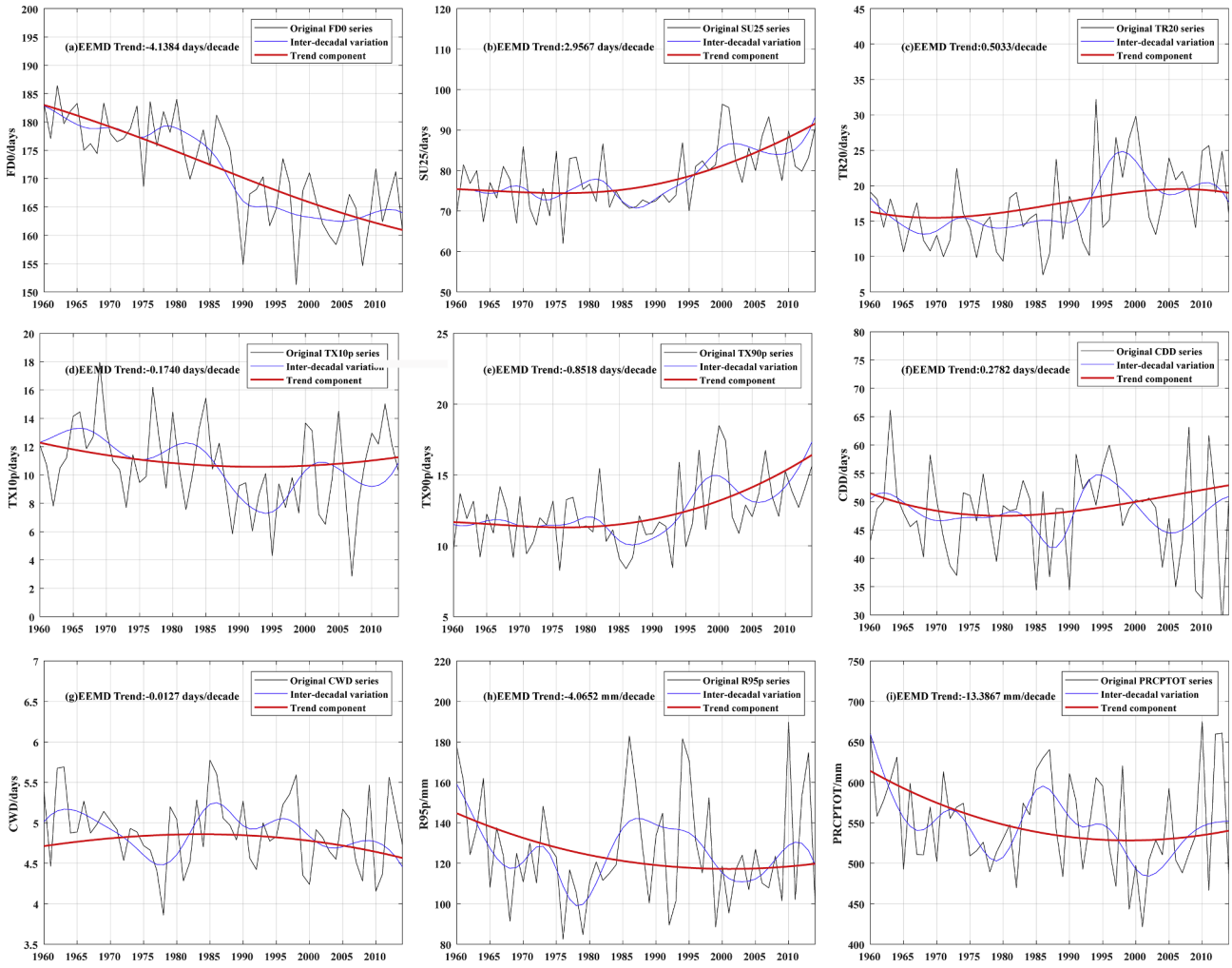

Fig. 2. Trend component and inter-decadal variations of extreme climate indices averaged over 70 stations in NEC during 1960–2014.

and significance tests are displayed beside each NEC graph. The results show that the 4-year period was dominant in the global wavelet spectrum of FD0, with significant wavelet power found in the 2-year and 2–5-year band around 1973–1976 and 1987–2003 (Fig. 3a). The wavelet power spectrum for the time series of SU25 and TX90P showed with 95% that the regions with high wavelet power were distributed in the 1.5-year and 3-year band, respectively, the continuous wavelet transform presented significant wavelet power in the 2–4-year band during 1963–1982 for both indices, with 1–5-year and 1–8-year bands around 1991–2014 in SU25 and TX90P, respectively (Fig. 3b, e). The global wavelet power spectrum of TR20 (Fig. 3c) showed that the 2-year and 6-year periods were significant at the 95% confidence level, with a 1–7-year band during 1973–2009. Fig. 3f shows the wavelet power in the 2–4-year band around 1961–1974, 1989–2003, and 2007–2012 and in the 4–6-year band during 1973–2003 of CDD. There were 4-year and 3.5-year significant periods, as shown in Fig. 3d and g, with 1–7-year and 1–6-year bands appearing throughout the study period for TX10P and CWD. A 4.2-year period was found in the global wavelet of R95pTOT and a 1–6-year band in 1982–2014 (Fig. 3h). PRCPTOT was dominated by 1.5- and 3-year periods, with a 1–5-year band found in 1984–2014 (Fig. 3i).

4.3. Spatial variability analysis

Fig. 4 indicates the numbers of stations showing specific trends, and Fig. 5 shows the spatial distribution of trends and averages of the extreme climate indices across NEC during 1960–2014. The results show that the regional averages of FD0 increased from southeast to northwest and Sen's slope of 70 stations was dominated by significant decreasing trends, with values ranging 0.606–6.522 days/decade. The trend slopes of FD0 in the central plains of Liaoning; eastern, southeast mountainous area of Jilin Province; and most of Heilongjiang were relatively high (Fig. 5a). For most of the stations, the value of TX10p was about 10 days, which was relatively uniform for many years. The lowest-value areas were in the Changbai Mountain region, whereas the highest-value areas were concentrated in Liaoning Province, which may have been affected by the local climate because of terrain conditions and the impact of sea-land interaction, respectively. Although the trends of 68 stations were decreasing, only 16 were statistically significant and scattered in the southeastern edges of the study area. The high-value regional averages of SU25 were found mainly in Liaoning Province, mid-western Jilin Province, and southwestern Heilongjiang Province, with a spatial distribution pattern of decrease from southwest to northeast. SU25 increased at a majority of meteorological stations, 54 of which passed the significance test and 47 of which showed a rate of increase of more than 2.000 days/decade. Notably, half of the Heilongjiang stations that showed large growth (3.333–4.571 days/decade; i.e., more than twice the rate of other stations) were located in the north (Fig. 5b). The average value of TR20 in Liaoning Province exceeded 30 days, whereas those of Jilin and Heilongjiang Provinces were 12 and 8.4 days, respectively. This indicates uneven spatial distribution of this index between northern and southern NEC, which is mainly related to the effects of the continental monsoon climate in the more temperate Liaoning Province. TR20 for all stations showed increasing trend, 31 of

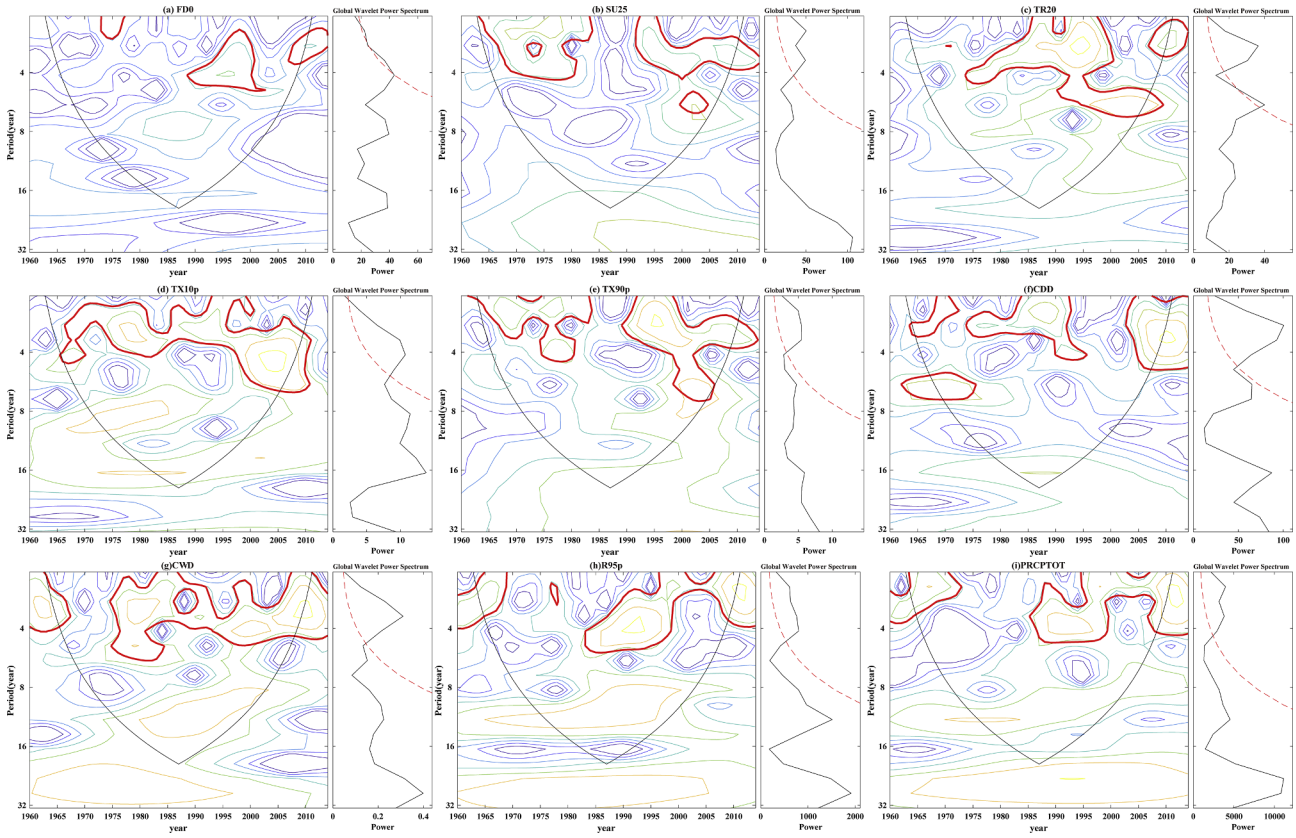

Fig. 3. Morlet wavelet transformation for extreme climate indices averaged over 70 stations in NEC during 1960–2014. The 'V'-shaped black line is the influence cone. The closed red lines are the periods of extreme indices. When the dashed line is smaller than the curve of the wavelet power spectrum, it indicates that the corresponding periods of a segment are significant at the 95% confidence level (Yang et al., 2017).

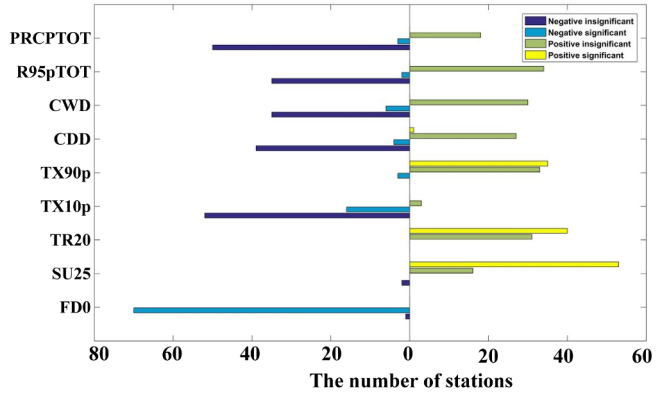

Fig. 4. Number of stations showing specific trends in extreme climate indices in NEC during 1960–2014.

which were significant, with higher trend slopes in the western regions and on the southwestern edges of the study area (Fig. 5c). The average TX90p was higher in Jilin Province, but more evenly distributed in the other two provinces. Nevertheless, 35 stations were characterized by significantly increasing trends in TX90p, 20 of which were in Heilongjiang Province (Fig. 5e). From the spatial distribution and trends of the extreme temperature indices, it can be seen that the increases in TX10p, TR20, and TX90p reduced the daily temperature difference, which led to a decrease in the number of frost days. Moreover, the increase in SU25 further prolonged the length of the spring and autumn seasons in NEC and increased the temperature of the region, which also accelerated the decrease in the number of frost days.

The regional averages of CDD were higher in the western region of NEC, which indicates that the climate in the western part of the study area was much dryer than that in the east. CDD showed positive trends at 28 stations and negative trends at 43 stations, but only 4 and 1 station(s), respectively, passed the significance test. The stations with rates of decrease in CDD of over 2.0 days/decade were all in Heilongjiang Province, with the exception of Changchun, for which Sen's slope was 2.6923 days/decade (Fig. 5f). The high-value areas in terms of average annual CWD were found in eastern Jilin Province, with 41 and 30 of the stations having downward and upward trends, respectively. However, only 6 were statistically significant (Fig. 5g). The average annual R95pTOT and PRCPTOT were more than 300 mm/year and 1000 mm/year, respectively, and had similar spatial distribution, wherein the values of the indices were higher in eastern Jilin Province. This demonstrates that other precipitation events in this region did not contribute to the total precipitation. In other words, extreme events in this region were becoming more intense, and the extreme precipitation events were mainly responsible for the total annual precipitation, which led to the reduction in total precipitation in most areas. For R95pTOT, 37 of the stations, which covered nearly half of NEC, showed decreases, and 53 stations had decreasing trends for PRCPTOT. However, similar to the other two precipitation indices, only a few stations passed the significance test, indicating unclear variations in the spatial patterns of extreme precipitation indices.

4.4. Future trends of the extreme climate indices

To predict the future trends of the extreme climate indices in NEC, the R/S analysis method was employed in this study to characterize the spatial variability and variation types of extreme climate indices, of which the results can be seen in Figs. 6 and 7.These figures demonstrate that more than half of the stations (58.6%) continued to decline in FD0, and the stations that switch from declining to rising are mainly located

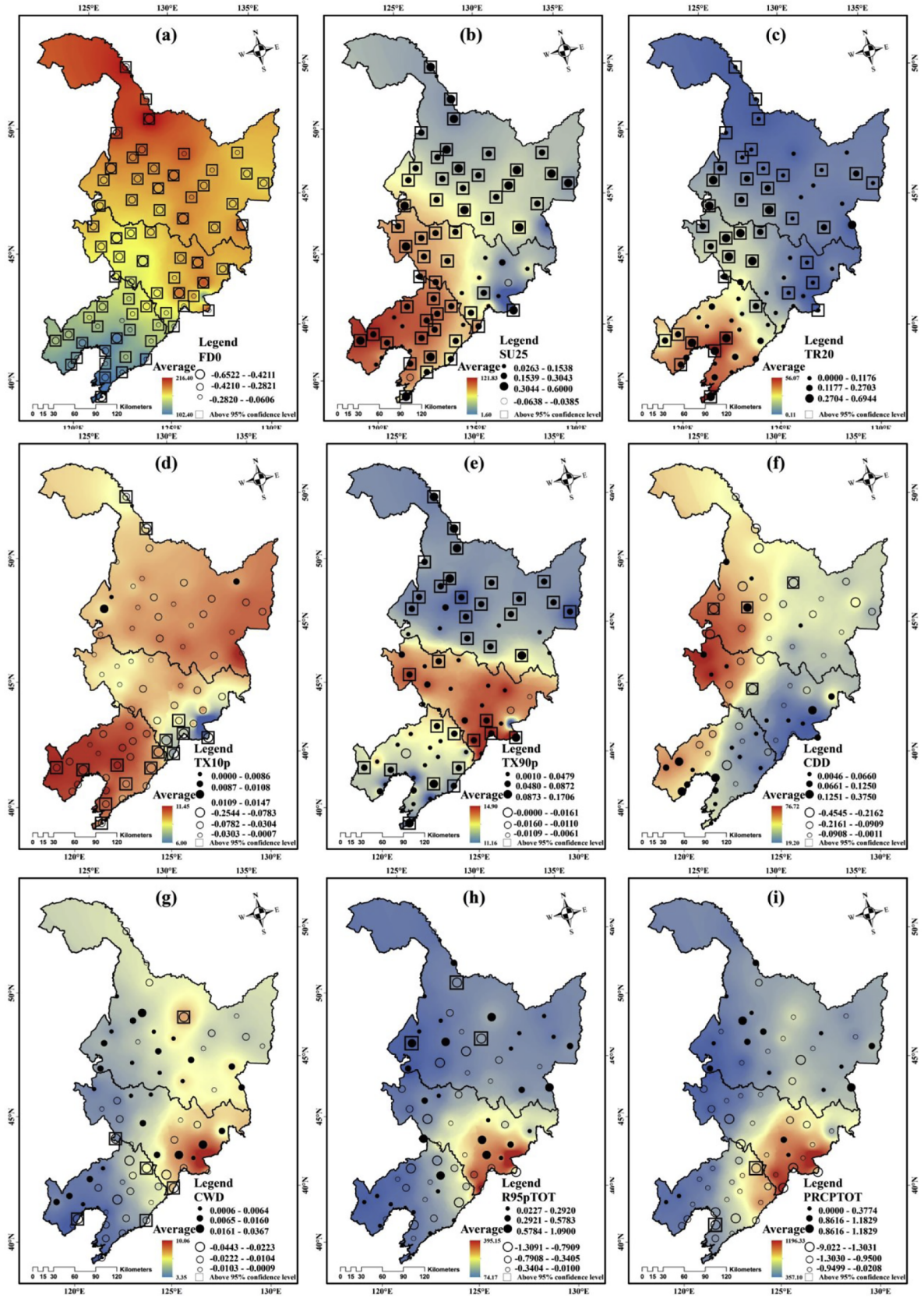

Fig. 5. Spatial distribution of trends and averaged extreme climate indices in NEC during 1960–2014.

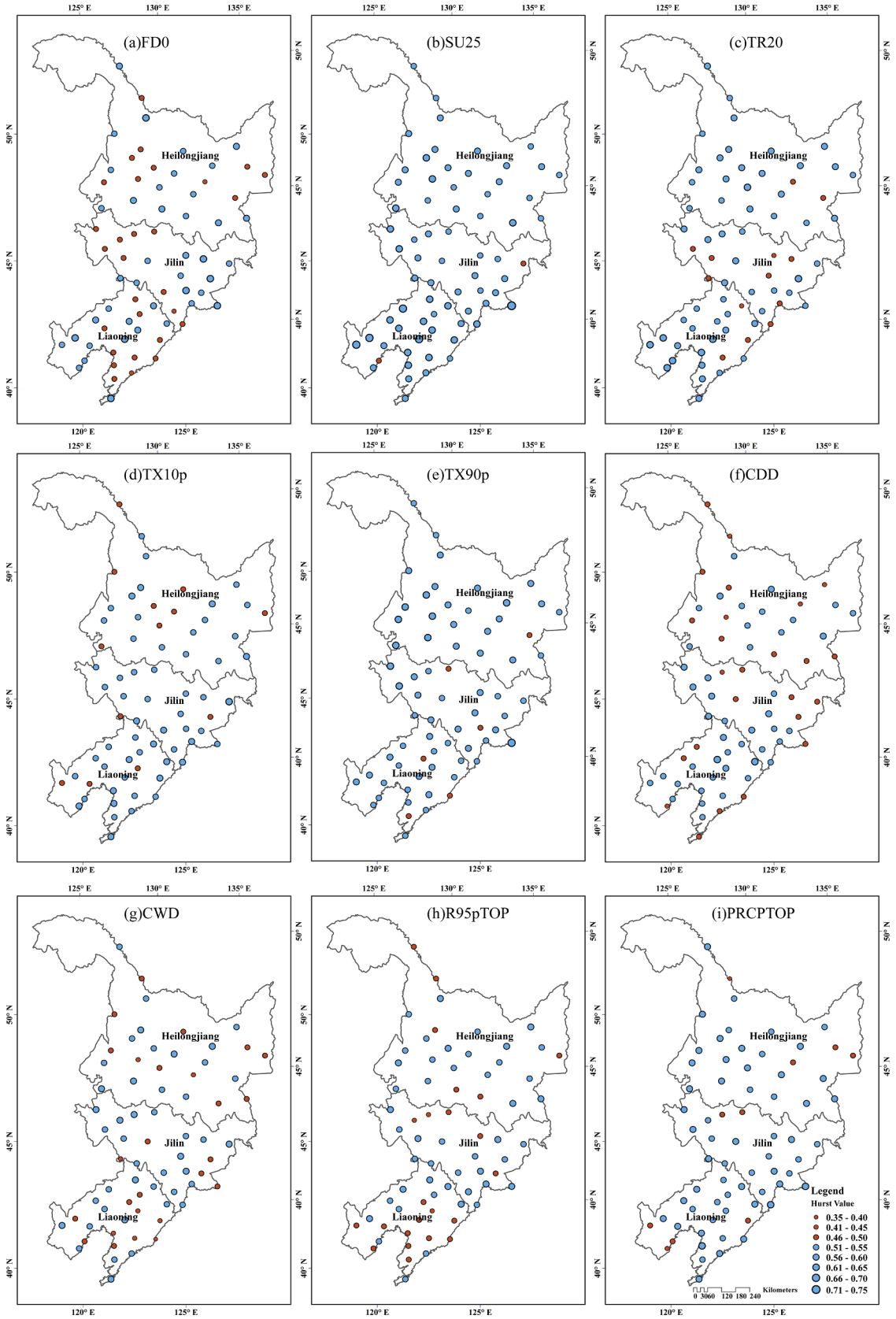

Fig. 6. Spatial distribution map of extreme climate indices in NEC based on the Hurst index.

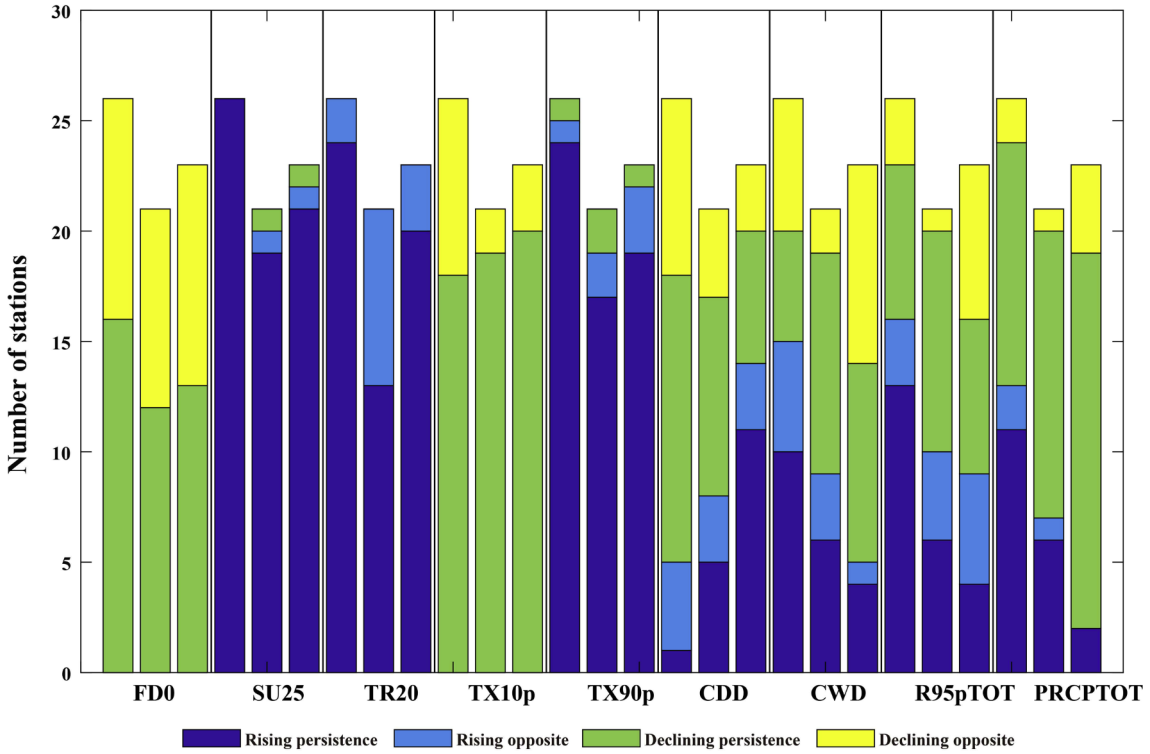

Fig. 7. Histogram of future change type of extreme climate indices for the three provinces of NEC Note: Histograms for each extreme climate index from left to right stand for Heilongjiang, Jilin, and Liaoning, respectively.

Table 3
Probability distributions with the highest goodness-of-fit for the extreme climate indices, and the *p* values for the Kolmogorov–Smirnov test.

Indicator	GEV	EV	EXP	POISS	NORM	GAMA	RAYL
FD0	*0.9702*	0.7354	0.0000	0.8804	0.0000	0.8804	0.0000
SU25	0.8804	0.7354	0.0000	0.0467	0.0000	*0.9979*	0.0148
TR20	0.9701	0.1964	0.7354	0.0002	0.0000	*0.9702*	0.0268
TX10p	*0.2931*	0.5716	0.0000	0.0000	0.0148	0.0467	0.0000
TX90p	*0.8804*	0.5716	0.0000	0.0001	0.2931	0.7354	0.0000
CDD	0.9999	0.8804	0.0001	0.2931	0.0000	*1.0000*	0.0268
CWD	*0.9702*	0.0268	0.0000	0.0148	0.5716	0.7354	0.0002
R95pTOT	*0.9702*	0.0040	0.0000	0.0001	0.0000	0.1964	0.0148
PRCPTOT	*1.0000*	0.0268	0.0000	0.0001	0.0000	0.7354	0.0009

Italic font indicates the selected probability distribution based on p values.

in the eastern region of NEC, western Jilin Province, and the central region of Heilongjiang Province. This shows that the temperature in these areas is susceptible to external factors, and the change process shows a characteristic of unstable decline. Most stations showed an increase trend in SU25, and the H value was generally higher, indicating a significant increase, only two stations in Jilin Province and Liaoning Province showed a declining trend, contrary to the current change trend. For TR20, 57 stations show an increasing trend, Heilongjiang and Liaoning have an obvious change trend, and the other stations showed the opposite trend of the present pattern, which showed a descending trend, indicating that there was a trend of decreasing daily range in the future. For TX10p, the values of the distribution were uniform, the distribution ranged between 0.48 and 0.61, and the majority of the stations showed a declining trend (57 stations), with stations with rising trends mainly located in Heilongjiang.85.7% stations of TX90p will continue to rise in the future, whereas only 6 stations were on the contrary at the present stage. The number of CDD-increased and -decreased stations is generally the same, but the Hurst index has many change types. The future trend of CWD has the opposite trend. R95pTOT also has four variation types, with the increased stations mainly located in Liaoning Province and Heilongjiang Province, the declining trend and the rising trend of the proportion of stations is 34/36. Whereas PRCPTOT has a significant change that mainly show a declining trend, with more than 70% stations of the rising trend and R95pTOT changes in the same trend. This shows that R95pTOT dominates the precipitation in these areas and the rising trend is mainly located in southwest Liaoning and eastern Heilongjiang Provinces. In summary, most of the extreme climate indices maintain their current change trend in the future; there was spatial difference in the variation type and Hurst value of each index. However, it is necessary to introduce the three-dimensional copula function to evaluate the joint occurrence probability because the Hurst method failed to measure the superposition effect among indices.

4.5. Trivariate joint return period analysis

As mentioned above, using individual indices to analyze the characteristics of extreme climate over time cannot fully depict the internal correlations between extreme temperature and precipitation. Therefore, to explain these characteristics and detect the regularity of extreme climate events in NEC, trivariate copula functions were introduced to calculate the trivariate joint probabilities and return periods of extreme climate indices. First, the probability distributions of the extreme climate indices in NEC were calculated using various marginal distribution functions, and then the Kolmogorov − Smirnov test was used to obtain the optimal fitting functions. The principle is that a larger *P* value indicates better fitting, with the marginal distribution function corresponding to the maximum value deemed the optimal distribution function. The results of these calculations are shown in Table 3; these results show that SU25, TR20, and CDD were GAMA distributed, and that the other six extreme weather indices followed GEV distribution. As shown in Fig. 8, the marginal distribution function mentioned above was more effective.

In this study, five extreme temperature indices and four extreme precipitation indices were selected, which could be combined into 84

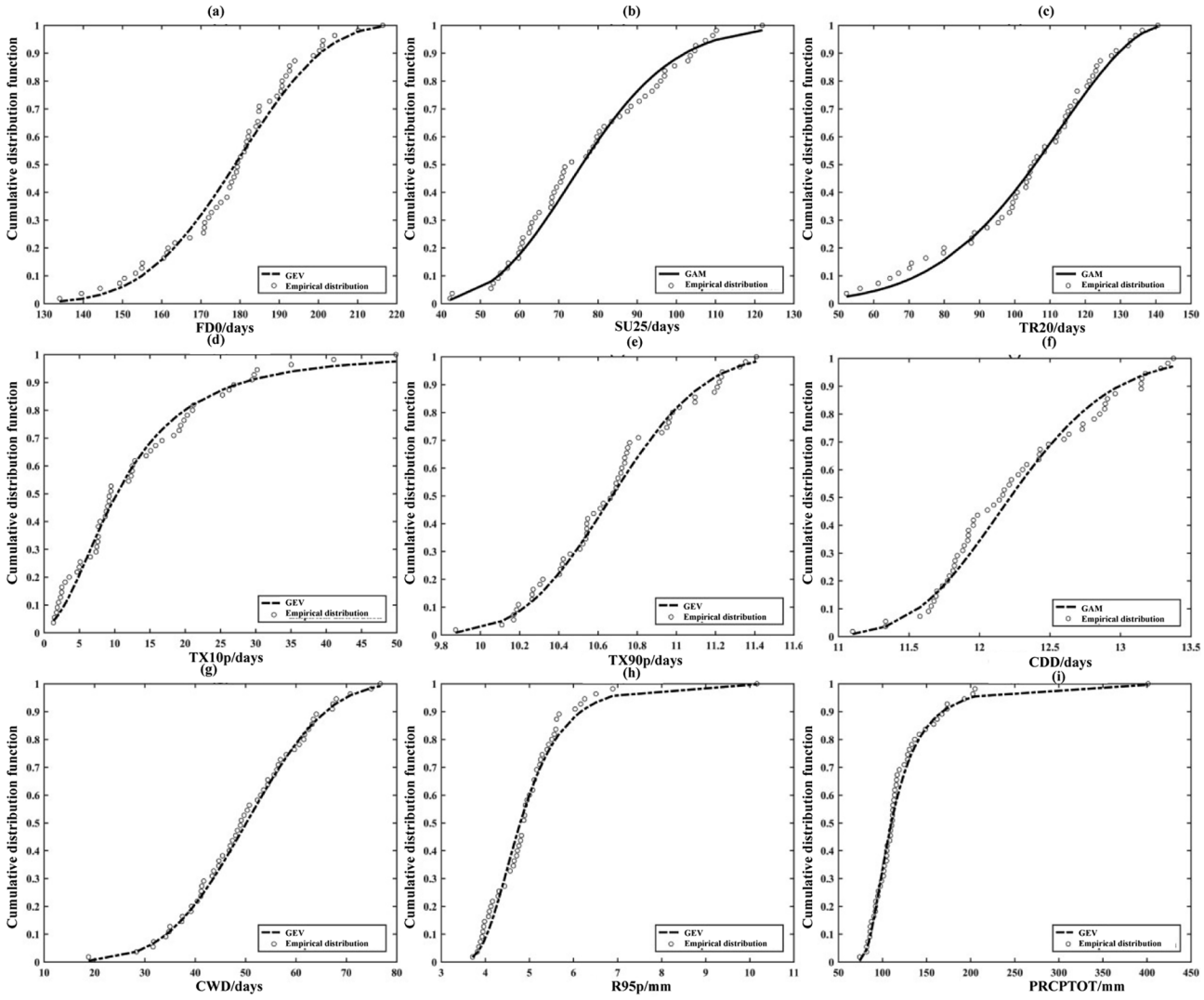

Fig. 8. Observed data and the fitted marginal distributions of the extreme climate indices averaged over 70 stations in NEC during 1960–2014.

trivariate combinations. However, some of these combinations lack full physical meaning. Consequently, nine combinations of the extreme climate indices were selected for calculation of trivariate copula functions. The minimum principle of the AIC criterion and the RMSE were used to select the optimal copula functions. The results are given in Table 4, and the trivariate joint return periods of the extreme climate indices averaged over 70 stations in NEC during 1960–2014 are shown in Fig. 9.

The spatial distribution of the conditional trivariate joint return periods of the extreme climate indices in NEC are shown in Fig. 10, where FD0:250, SU25:120, TR20:120, TX10p:20, TX90p:25, CDD:160, CWD:25, R95pTOT:1000, and PRCPTOT:1500. The results show that under the specified conditions, the return period of each combination of indices showed a significantly different spatial distribution pattern from those of the other combinations. For SU25&TR20&TX90p, long return periods were located in southeastern Jilin and northeastern Liaoning Provinces, which correspond to periods of over 200 and 1000 years, respectively. The spatial distribution pattern showed a decline from southeast to northwest, which indicates that the hazard level gradually increases and that the night-time temperature in the southeastern mountainous areas is more sensitive to climate warming. Long return periods of FD0&SU25&TX10p, in excess of 100 years, were mainly located in southeastern Heilongjiang Province. Short return periods mainly within 1–14 years were found throughout most of Liaoning and the mid-western regions of Jilin Province, which indicates that those low-latitude regions and traditionally arid zones are vulnerable to the continental monsoon and maritime climates. The joint return period of FD0&CWD&PRCPTOT was mainly around 1–2 years, and the most hazardous areas were located in southeastern Jilin and the mountainous area of northeastern Liaoning Province, which indicates that those areas have colder winters and higher annual precipitation than other regions of NEC. FD0&TX10p&CDD and FD0&SU25&TX10p showed similar spatial distributions, meaning that the number of consecutive dry days determines the length of summer. The most hazardous areas were located in Liaoning and western Jilin Provinces, which are therefore characterized by long winters, low temperatures, and less precipitation, as well as higher probability of the occurrence of low temperatures and droughts relative to other regions. Nevertheless, the joint return period was slightly lower for the former than for the latter combination, which indicates that for SU25 and CDD, with the synchronization phenomenon between temporal and spatial changes, the probability of CDD extension increases when SU25 is extended. The least hazardous areas were mainly located in eastern Jilin and northeastern Liaoning Provinces, where the joint return period was higher than 1000 years, which indicates that the probabilities of high summer temperatures and water shortages were small. The longest return periods of SU25&TX90p& R95pTOT were mainly distributed in eastern Jilin and eastern Heilongjiang Provinces, with a joint return period of above 385.5 years,

Table 4
Selection of copula function based on the AIC and RMSE values.

Extreme climate index combination	Copula function	RMSE	AIC
SU25&TR20&TX90p	Clayton	0.242029	−63.7746
	Frank	0.235531	−65.0746
	Gumbel	0.236309	−64.9173
FD0&SU25&TX10p	*Clayton*	0.217988	−68.7723
	Frank	0.218911	−68.5706
	Gumbel	0.219636	−68.4125
FD0&CWD&PRCPTOT	Clayton	0.167699	−81.3015
	Frank	0.165032	−82.0675
	Gumbel	0.167699	−81.3015
FD0&TX10p&CDD	Clayton	0.232278	−65.7392
	Frank	0.235115	−65.1592
	Gumbel	0.236681	−64.8419
SU25&TR20&CDD	Clayton	0.238359	−64.5046
	Frank	0.233485	−65.4916
	Gumbel	0.236434	−64.8918
SU25&TX90p&R95pTOT	Clayton	0.174845	−79.3078
	Frank	0.180285	−77.8445
	Gumbel	0.174846	−79.3079
TR20&CWD&R95pTOT	Clayton	0.175969	−79.0021
	Frank	0.173974	−79.5466
	Gumbel	0.175968	−79.0022
TR20&TX90p&CDD	Clayton	0.089804	−111.136
	Frank	0.095349	−108.275
	Gumbel	0.089805	−111.137
CWD&R95pTOT&PRCPTOT	Clayton	0.192337	−74.753
	Frank	0.186697	−76.1749
	Gumbel	0.190857	−75.1222

Italic font indicates the selected copula function based on values of the AIC and RMSE.

which indicated that the probability of high temperatures and heavy rainfall was smaller than it was in other regions. The spatial distribution of TR20&CWD&R95pTOT was the opposite of that shown in Fig. 10c and i, which was mainly distributed in northwestern Liaoning, Jilin, and Heilongjiang Provinces. These areas are traditionally drought-prone, with high probabilities of high temperatures and heavy precipitation. This also shows that persistent precipitation reduces nighttime temperatures, which is conducive to the development of frost days. These results indicate that the intensity of extreme precipitation events increased. The joint return period of TR20&TX90p&CDD increased gradually from south to north, which indicates that the probability of high temperatures, heat waves, and droughts gradually decreased. The joint return period was more than 10,000 years across most of Heilongjiang Province, which indicates that the specified conditions far exceeded the historical maximum of this region; therefore, the occurrence of these conditions is essentially impossible in this region. The spatial distribution of CWD&R95pTOT&PRCPTOT was similar to that shown in Fig. 10c, with a return period of 1–2 years. Short joint return periods were found in southeastern Jilin and northeastern Liaoning Provinces, and longer joint return periods were found in northwestern Liaoning, western Jilin, and Heilongjiang Provinces, which correspond to traditionally drought-prone areas. In summary, global warming has exacerbated the intensity of extreme precipitation events, i.e., the intensity of single extreme precipitation events has increased, which has resulted in an increase in the probability of flooding. Moreover, the probability of the occurrence of extreme precipitation events in arid areas has increased substantially. Heat waves have occurred in the region since the onset of climate warming, and this phenomenon will become more frequent in the future. Fig. 10a and h show that the increasing temperature throughout the day has led to the phenomenon of consecutive dryness, meanwhile the emergence of this probability event has been exacerbated by the increasing number of summer days. We also found that there is a large probability of occurrence of abrupt alternation between droughts and floods in the western region by comparing the spatial distribution patterns in Fig. 10.

5. Discussion

The temperature has increased in most regions around the world, including the eastern United States, northern Europe, western African, and East Asia. (IPCC, 2014), in particular, the temperature increase in high latitudes is greater than in low latitudes (Stocker et al., 2013). Over 70% of the global land area showed a significant decrease in the annual occurrence of cold nights and a significant increase in the annual occurrence of warm nights (Alexander et al., 2006). In this study, we found that the NEC has experienced significant temperature rise; climate warming and extreme high temperatures have increased the probability of extreme drought and heat waves in this region. The results revealed that the temperature in NEC shows an upward trend, whereas precipitation has decreased, which indicates that this area tends to be relatively warm and dry. Compared with the variation of national average extremes, FD0 and SU25 are faster than the national and western regions, by analysing variation of TX10p and TX90p, we can see that the temperature change during the day is smaller than the national and Loess Plateau. The change rate of FD0 and SU25 are ascending and descending, which shows that the night time temperature of NEC becomes lower and the temperature difference between day and night becomes larger than those of the whole country and the Loess Plateau. For the extreme precipitation, the intensity in the NEC decays more rapidly than in other areas, indicating that warm events are more frequent and stronger and the NEC will experience more intensified extreme precipitation events (Fang et al., 2016; Chen and Sun, 2015). These findings are consistent with the global pattern of climate change in which arid climates are becoming drier and humid climates are becoming increasingly moist (Greve et al., 2014).

In this study, the EEMD method was used to analyze regional nonlinear variation of extreme climate indices in NEC, and the trends of change detected were similar to those reported by Yu and Li (2015), although in their study, the overall change was determined by means of linear regression analysis. However, we also found that the trends of indices with larger inter-annual changes differ substantially between the two studies, because the EEMD method overcomes the aliasing of anomalous events and the inherent patterns of meteorological data and can therefore more accurately represent chronological changes and the general trends of extreme climate change in NEC. The Sen's slope estimator method and the Morlet continuous wavelet transform method were applied in the current study to analyze the extreme climate indices separately. Our findings indicate that the trends of extreme temperature and precipitation events were consistent with those reported by other scholars (Du et al., 2013a,b; Wang et al., 2016a,b). Most previous studies have focused on the calculation of single probabilities and the return periods of indices, which have been extended to two or more dimensions in recent years (Chang et al., 2016; Chen et al., 2016; She et al., 2016). However, even the calculation of two-dimensional joint probability was focused mainly on extreme precipitation or extreme temperature indices. The superposition effect of extreme temperature and precipitation will seriously affect the evaluation of the severity of extreme events. The most reliable assessment of the severity and duration of extreme climate events will be achieved by considering indices of both extreme temperature and extreme precipitation. The trivariate copula functions were applied to investigate the combination of extreme climate events in NEC and have revealed the spatial distributions of multiple combinations of extreme indices in terms of the joint return period. In this study, the intrinsic correlations between the climatic system and extreme climate indices in this region were explored preliminarily (Table 5).

Extreme climate change is constrained by many factors, including global warming and violently anthropogenic influence on the frequency

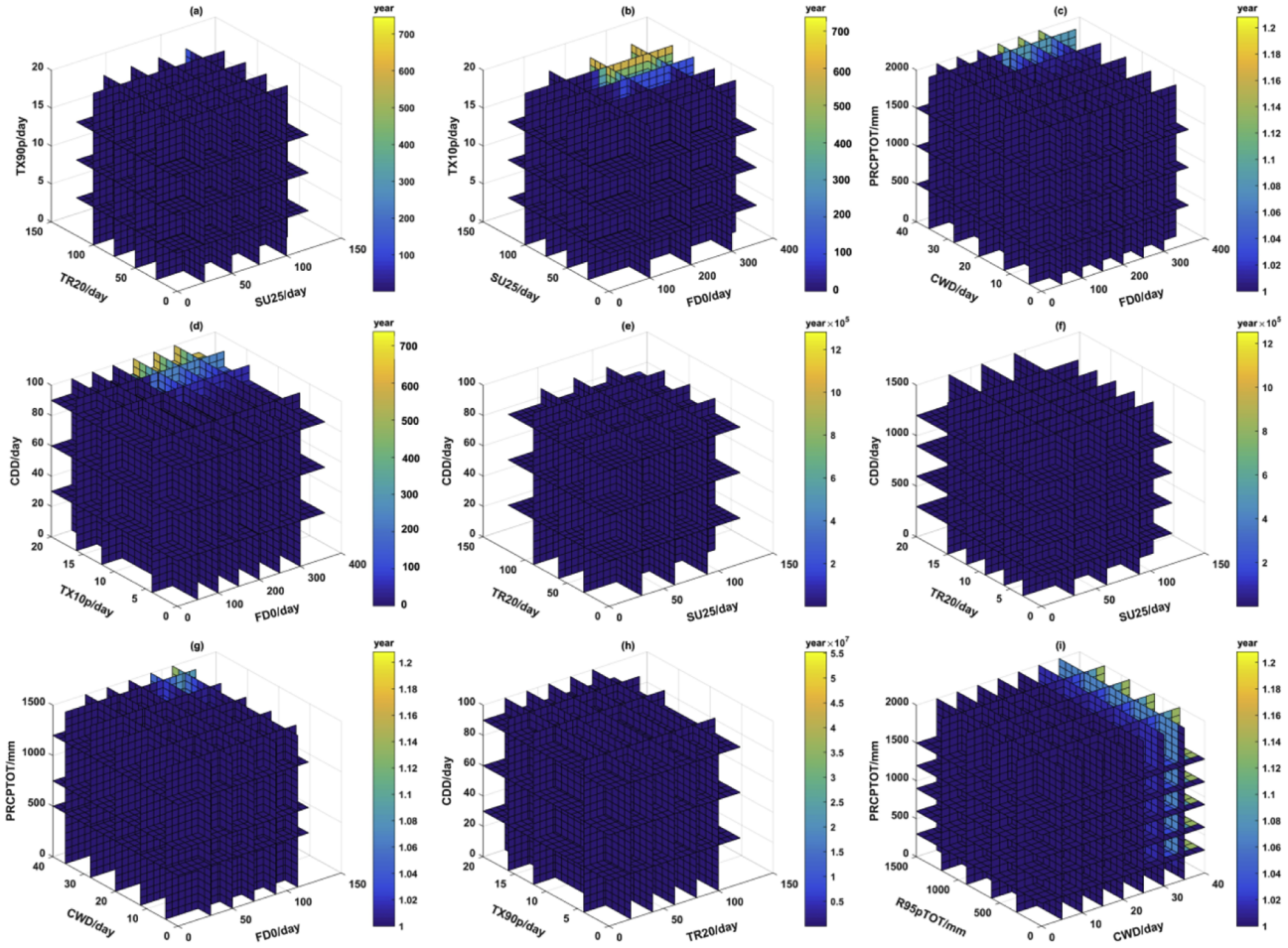

Fig. 9. Trivariate joint return periods of the extreme climate indices averaged over 70 stations in NEC during 1960–2014.

of extreme temperature and precipitation events (He and Wang, 2016). However, Lu et al. (2016) have demonstrated that anthropogenic influence explains more than 90% of the observed changes in the frequency of temperature extremes; therefore, it is particularly necessary to deal with climate change and unreasonable human activities. The central region of NEC is an important black earth belt in China and the world, which makes it an important grain production base in China. To increase maize yield, local farmers converted to growing late maturing varieties, but frost injury and flood or drought disasters greatly reduce yield. Owing to the increase of extreme climate events, those regions will face drier conditions and drought disaster may occur. In response to climate change, China has adopted a series of measures to deal with it. For example, the New Climate Change Commitments of the United States and China state that China will promote non-fossil fuel energy generation for the supply of 20 percent of the country's energy needs by 2030, which will require between 800 GW and 1000 GW of nuclear, wind, solar, and other zero-emission power generation by 2030 (Economy, 2007). Meanwhile, the Paris Climate Agreement states that compared to 2005, the carbon dioxide emissions per unit of GDP in 2030 should drop by 60%–65% in China, non-fossil fuel energy should account for about 20% of the primary energy consumption, and forest reserves should have increased by about 4.5 billion cubic meters (Zhang et al., 2017). In general, coping with global warming requires the joint efforts of all global sectors.

Overall, in this study, the spatiotemporal variation and characteristics of extreme climate indices in NEC were studied using various methods, and useful information was obtained, which potentially is useful for natural disaster prevention and mitigation. However, certain shortcomings remain, such as the sparseness of meteorological stations, which limit the accuracy of evaluating spatial variation and thus need to be improved. Moreover, in this study, only three kinds of copula functions were compared and analyzed. If as many functions as possible are introduced to extract the optimal copula functions, the accuracy of the joint return periods will undoubtedly be improved. In addition, the emergence conditions of floods and droughts are highly complex, based on the theory of the formation of these natural disasters; therefore, whether changes in extreme climate indices are directly related to flood and drought disasters is a direction for future research.

6. Conclusion

This study aims to detect the variation characteristics and periodicity of individual indices, and the joint probability and return periods of the extreme climate indices in NEC during 1960–2014.The main conclusions are as follows.

(1) The extreme warm indices had increasing trends, whereas extreme cold indices had decreasing trends, as did the extreme precipitation indices, excluding CDD. Since 1990, the NEC has become more and more warm and dry in most areas.
(2) Most of the extreme temperature indices shared a significant 3, 3.5, and 4 years band, whereas the extreme cold indices and extreme precipitation indices had relatively longer periods of 3, 3.5, and 4 years. The extreme climate indices showed strong periodic oscillation variations in their continuous wavelet transformation.
(3) FD0, SU25, TR20, and TX90p had the most significant trends, at 69, 54, 40, and 34 meteorological stations, respectively. With the exception of one station, FD0 decreased significantly in NEC, and

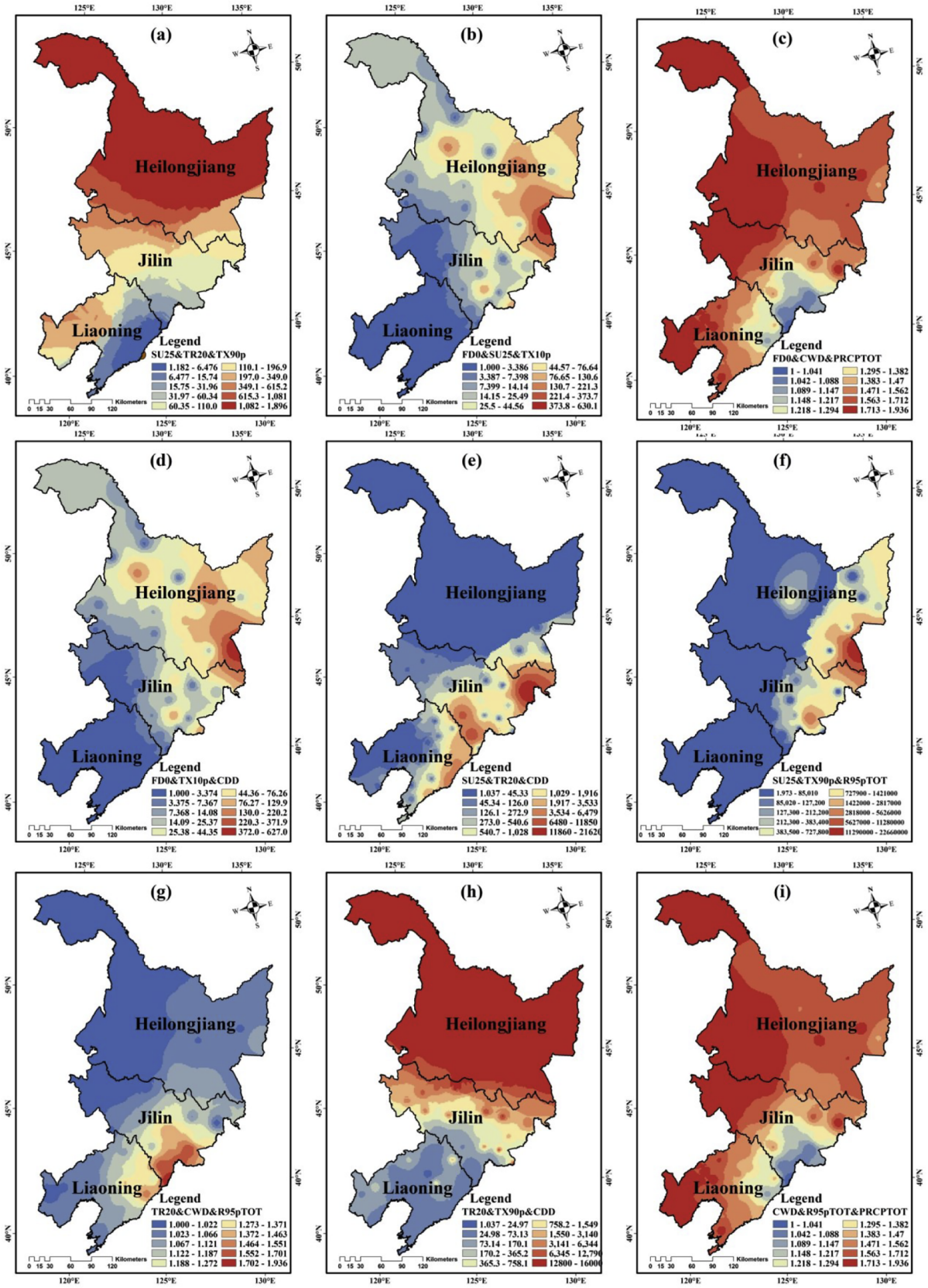

Fig. 10. Spatial distribution of the conditional trivariate joint return period of the extreme climate index combinations for NEC.

Table 5
Trends of extreme climate indices from this study and other works.

Indicator	NEC	Tibetan Plateau	Loess Plateau	China	Japan	Global
FD0	−4.14	−4.00	−3.22	−3.48	–	–
SU25	2.96	0.94	2.76	2.69	–	–
TR20	0.50	0.41	1.24	2.47	–	–
TX10p	−0.17	1.43	−2.71	−3.26	–	−0.62
TX90p	0.85	–	2.60	5.22	–	0.89
CDD	0.28	–	1.95	−1.22	2.37	−0.55
CWD	−0.01	–	−0.5	–	−1.78	–
R95pTOT	−4.07	2.4	−3.5	4.06	0.83	4.07
PRCPTOT	−13.39	–	15.0	3.21	1.5	10.59
Data source	This study	You et al. (2018)	Sun et al. (2016)	You et al. (2011)	Duan et al. (2015)	Alexander et al. (2006)

TX10p decreased significantly in the southeastern and northeastern regions of NEC. The extreme precipitation indices CDD, CWD, R95pTOT, and PRCPTOT did not significantly change during 1960–2014. Only a few stations scattered in various areas showed significant variationin these indices; meanwhile, the vast majority of climate indices maintained their current change trends in the future.

(4) By using the optimal copula functions, we found that the probabilities of cold winters and excessive precipitation in southeastern Jilin and northeastern Liaoning Provinces are higher than in other regions. Both high temperatures and heavy precipitation are more frequent in northwestern Liaoning, western Jilin, and Heilongjiang Provinces.

Acknowledgements

This study was supported by the National Natural Science Foundation of China under Grant (No. 41571491), China Special Fund for Meteorological Research in the Public Interest (No. 2015001), the Fundamental Research Funds for the Central Universities (No. 2412016KJ046), National Science Foundation for Young Scientists of China (No. 41807507) and the Science and Technology Development Plan projects of Inner Mongolia (No. 201502095). The authors are grateful to the anonymous reviewers for their insightful and helpful comments to improve the manuscript.

References

Agarwal, A., Maheswaran, R., Kurths, J., Khosa, R., 2016a. Wavelet Spectrum and self-organizing maps-based approach for hydrologic regionalization-a case study in the western United States. Water. Resour. Manage. 30 (12), 4399–4413.
Agarwal, A., Maheswaran, R., Sehgal, V., Khosa, R., Sivakumar, B., Bernhofer, C., 2016b. Hydrologic regionalization using wavelet-based multiscale entropy method. J. Hydrol. 538, 22–32.
Alexander, L.V., Zhang, X., Peterson, T.C., et al., 2006. Global observed changes in daily climate extremes of temperature and precipitation. J. Geophys. Res-Atmos. 111 (D5), 1042–1063.
Bahinipati, C.S., Venkatachalam, L., 2016. Role of climate risks and socio-economic factors in influencing the impact of climatic extremes: a normalisation study in the context of Odisha. India. Reg. Environ. Change 16 (1), 177–188.
Barlow, K.M., Christy, B.P., O'Leary, G.J., Riffkin, P.A., Nuttall, J.G., 2015. Simulating the impact of extreme heat and frost events on wheat crop production: a review. Field Crops Res. 171, 109–119.
Cabras, S., Castellanos, M.E., Gamerman, D., 2011. A default Bayesian approach for regression on extremes. Stat. Model. 11 (6), 557–580.
Chang, J., Li, Y., Wang, Y., Yuan, M., 2016. Copula-based drought risk assessment combined with an integrated index in the Wei River Basin, China. J. Hydrol. 540, 824–834.
Chen, H., Sun, J., 2015. Changes in climate extreme events in China associated with warming. Int. J. Climatol. 35 (10), 2735–2751.
Chen, Y.D., Zhang, Q., Xiao, M., Singh, V.P., Zhang, S., 2016. Probabilistic forecasting of seasonal droughts in the Pearl River basin, China. Stoch. Env. Res. Risk. A 30 (7), 2031–2040.
Du, H., Wu, Z., Li, M., Jin, Y., Zong, S., Meng, X., 2013a. Characteristics of extreme daily minimum and maximum temperature over Northeast China, 1961–2009. Theor. Appl. Climatol. 111 (1–2), 161–171.
Du, H., Wu, Z., Zong, S., Meng, X., Wang, L., 2013b. Assessing the characteristics of extreme precipitation over northeast China using the multifractal detrended fluctuation analysis. J. Geophys. Res-Atmos. 118 (12), 6165–6174.
Duan, W., He, B., Takara, K., et al., 2015. Changes of precipitation amounts and extremes over Japan between 1901 and 2012 and their connection to climate indices. Clim. Dynam. 45 (7–8), 2273–2292.
El-Zein, A., Tonmoy, F.N., 2015. Assessment of vulnerability to climate change using a multi-criteria outranking approach with application to heat stress in Sydney. Ecol. Indic. 48 (Supplement C), 207–217.
Fang, S., Qi, Y., Yu, W., et al., 2016. Change in temperature extremes and its correlation with mean temperature in mainland China from 1960 to 2015. Int. J. Climatol. 37 (10), 3910–3918.
Farge, M., 1992. Wavelet transforms and their applications to turbulence. Annu Rev Fluid Mech. 24 (1), 395–458.
Farajzadeh, M., Oji, R., Cannon, A.J., Ghavidel, Y., Bavani, A.M., 2015. An evaluation of single-site statistical downscaling techniques in terms of indices of climate extremes for the Midwest of Iran. Theor. Appl. Climatol. 120 (1–2), 377–390.
Gao, T., Shi, X., 2016. Spatio-temporal characteristics of extreme precipitation events during 1951–2011 in Shandong, China and possible connection to the large scale atmospheric circulation. Stoch. Env. Res. Risk. A 30 (5), 1421–1440.
Ganguli, P., Reddy, M.J., 2013a. Analysis of ENSO-based climate variability in modulating drought risks over western Rajasthan in India. J. Earth. Syst. Sci. 122 (1), 253–269.
Ganguli, P., Reddy, M.J., 2013b. Probabilistic assessment of flood risks using trivariate copulas. Theor. Appl. Climatol. 111 (1–2), 341–360.
García-Cueto, O.R., Cavazos, M.T., de Grau, P., Santillán-Soto, N., 2014. Analysis and modeling of extreme temperatures in several cities in northwestern Mexico under climate change conditions. Theor. Appl. Climatol. 116 (1–2), 211–225.
Gocic, M., Trajkovic, S., 2013. Analysis of changes in meteorological variables using Mann-Kendall and Sen's slope estimator statistical tests in Serbia. Global. Planet Change 100, 172–182.
Graham, J.H., et al., 2012. The effects of drought and disturbance on the growth and developmental instability of loblolly pine (Pinus taeda L.). Ecol. Indic. 20 (Supplement C), 143–150.
Greve, P., Orlowsky, B., Mueller, B., Sheffield, J., Reichstein, M., Seneviratne, S.I., 2014. Global assessment of trends in wetting and drying over land. Nat. Geosci. 7 (10), 716–721.
Goupillaud, P., Grossman, A., Morlet, J., 1984. Cycle-octave and related transforms in seismic signal analysis. Geoexploration 23 (1), 85–102.
He, S., Wang, H., 2016. Linkage between the East Asian January temperature extremes and the preceding Arctic Oscillation. Int. J. Climatol. 36 (2), 1026–1032.
Hu, Q., Pan, F., Pan, X., et al., 2016. Trends in agricultural heat and solar radiation resources in Northeast China: A multistage spatio-temporal analysis. Int. J. Climatol. 36 (6), 2461–2468.
IPCC, 2014. Impacts, Adaptation, and Vulnerability. Part B: Regional Aspects. Contribution of Working Group II to the Fifth Assessment Report of the Intergovernmental Panel on Climate Change. Cambridge Univesity Press, Cambridge, United Kingdom and New York.
Keggenhoff, I., Elizbarashvili, M., Amiri-Farahani, A., King, L., 2014. Trends in daily temperature and precipitation extremes over Georgia, 1971–2010. Weather Clim. Extremes 4, 75–85.
Kreft, S., Eckstein, D., Junghans, L., Kerestan, C., Hagen, U., 2014. Global climate risk index 2015: who suffers most from extreme weather events? weather-related loss events in 2013 and 1994 to 2013.
Lesk, C., Rowhani, P., Ramankutty, N., 2016. Influence of extreme weather disasters on global crop production. Nature 529, 84–87.
Li, Z., Yang, P., Tang, H., Wu, W., Yin, H., Liu, Z., Zhang, L., 2014. Response of maize phenology to climate warming in Northeast China between 1990 and 2012. Reg. Environ. Change 14 (1), 39–48.
Li, J., Zhang, Q., Chen, Y.D., Singh, V.P., 2015. Future joint probability behaviors of precipitation extremes across China: Spatiotemporal patterns and implications for flood and drought hazards. Global. Planet Change 124, 107–122.
Lin, Y., Feng, Z., Wu, W., Yang, Y., Zhou, Y., Xu, C., 2017. Potential impacts of climate change and adaptation on Maize in Northeast China. Agron. J. 109 (4), 1476–1490.
Ma, M., Song, S., Ren, L., Jiang, S., Song, J., 2013. Multivariate drought characteristics using trivariate Gaussian and Student t copulas. Hydrol Process. 27 (8), 1175–1190.
Miao, C., Sun, Q., Duan, Q., Wang, Y., 2016. Joint analysis of changes in temperature and precipitation on the Loess Plateau during the period 1961–2011. Clim. Dynam. 47 (9–10), 3221–3234.
Mutiibwa, D., Vavrus, S.J., McAfee, S.A., Albright, T.P., 2015. Recent spatiotemporal patterns in temperature extremes across conterminous United States. J. Geophys. Res-Atmos. 120 (15), 7378–7392.
Narasimha, R., Bhattacharyya, S., 2010. A wavelet cross-spectral analysis of solar–ENSO–rainfall connections in the Indian monsoons. Appl. Comput. Harmon. A 28 (3), 285–295.
Nicolay, S., Mabille, G., Fettweis, X., Erpicum, M., 2009. 30 and 43 months period cycles found in air temperature time series using the Morlet wavelet method. Clim. Dynam. 33 (7–8), 1117–1129.
Qian, C., Ren, G., Zhou, Y., 2016. Urbanization effects on climatic changes in 24 particular timings of the seasonal cycle in the middle and lower reaches of the Yellow River. Theor. Appl. Climatol. 124 (3–4), 781–791.
Peng, J., Liu, Z., Liu, Y., Wu, J., Han, Y., 2012. Trend analysis of vegetation dynamics in Qinghai-Tibet Plateau using Hurst Exponent. Ecol. Indic. 14 (1), 28–39.
Ruml, M., Gregorić, E., Vujadinović, M., Radovanović, S., Matović, G., Vuković, A., Stojičić, D., 2017. Observed changes of temperature extremes in Serbia over the

period 1961–2010. Atmos. Res. 183, 26–41.
Sang, Y.F., 2013. A review on the applications of wavelet transform in hydrology time series analysis. Atmos. Res. 122, 8–15.
Sen, P.K., 1968. Estimates of the regression coefficient based on Kendall's tau. J. Am. Stat. Assoc. 63 (324), 1379–1389.
She, D., Mishra, A.K., Xia, J., Zhang, L., Zhang, X., 2016. Wet and dry spell analysis using copulas. Int. J. Climatol. 36 (1), 476–491.
Shrestha, A.B., Bajracharya, S.R., Sharma, A.R., Duo, C., Kulkarni, A., 2016. Observed trends and changes in daily temperature and precipitation extremes over the Koshi river basin 1975–2010. Int. J. Climatol. 37 (2), 1066–1083.
Saghafian, B., Mehdikhani, H., 2014. Drought characterization using a new copula-based trivariate approach. Nat. Hazards 72 (3), 1391–1407.
Sklar, K., 1959. Fonctions de repartition à n Dimensions et Leura Marges. Publ. Inst. Stat. Univ. Paris 8, 229–231.
Stocker, T.F., et al., 2013. Climate Change 2013: The Physical Science Basis. Intergovernmental Panel on Climate Change, Working Group I Contribution to the IPCC Fifth Assessment Report (AR5). Cambridge University Press, New York.
Sun, W., Mu, X., Song, X., et al., 2016. Changes in extreme temperature and precipitation events in the Loess Plateau (China) during 1960–2013 under global warming. Atmos. Res. 168, 33–48.
Tamaddun, K.A., Kalra, A., Bernardez, M., Ahmad, S., 2017. Multi-scale correlation between the western US snow water equivalent and ENSO/PDO using wavelet analyses. Water. Resour. Manage. 1–15.
Torrence, C., Compo, G.P., 1998. A practical guide to wavelet analysis. BAMS 79, 61–78.
van Wilgen, N.J., Goodall, V., Holness, S., Chown, S.L., McGeoch, M.A., 2016. Rising temperatures and changing rainfall patterns in South Africa's national parks. Int. J. Climatol. 36 (2), 706–721.
Wang, C., Ren, X., Li, Y., 2015. Analysis of extreme precipitation characteristics in low mountain areas based on three-dimensional copulas—taking Kuandian County as an example. Theor. Appl. Climatol. 128 (1–2), 169–179.
Wang, L., Wu, Z., Wang, F., Du, H., Zong, S., 2016a. Comparative analysis of the extreme temperature event change over Northeast China and Hokkaido, Japan from 1951 to 2011. Theor. Appl. Climatol. 124 (1–2), 375–384.
Wang, P., Zhang, Z., Chen, Y., Wei, X., Feng, B., Tao, F., 2016b. How much yield loss has been caused by extreme temperature stress to the irrigated rice production in China? Climatic Change 134 (4), 635–650.
Wang, Q.X., Wang, M.B., Fan, X.H., Zhang, F., Zhu, S.Z., Zhao, T.L., 2017. Trends of temperature and precipitation extremes in the Loess Plateau Region of China, 1961–2010. Theor. Appl. Climatol. 129 (3–4), 949–963.
Wen, X., Feng, Q., Deo, R.C., Wu, M., Si, J., 2016. Wavelet analysis–artificial neural network conjunction models for multi-scale monthly groundwater level predicting in an arid inland river basin, northwestern China. Hydrol. Res. 48 (6), 1710–1729.
Wu, Z., Huang, N.E., 2009. Ensemble empirical mode decomposition: a noise-assisted data analysis method. Adv. Adaptive Data Anal. 1 (1), 1–41.
Yang, P., Xia, J., Zhang, Y., Hong, S., 2017. Temporal and spatial variations of precipitation in Northwest China during 1960–2013. Atmos. Res. 183, 283–295.
Yu, Z., Li, X., 2015. Recent trends in daily temperature extremes over northeastern China (1960–2011). Quatern. Int. 380, 35–48.
You, Q., Kang, S., Aguilar, E., et al., 2011. Changes in daily climate extremes in China and their connection to the large scale atmospheric circulation during 1961–2003. Clim. Dynam. 36 (11–12), 2399–2417.
You, Q., Jiang, Z., et al., 2018. Simulation of temperature extremes in the Tibetan Plateau from CMIP5 models and comparison with gridded observations. Clim. Dynam. 51 (1–2), 355–369.
Zeng, W., Yu, Z., Wu, S.H., Qin, J.B., 2016. Changes in annual, seasonal and monthly precipitation events and their link with elevation in Sichuan province, China. Int. J. Climatol. 36 (5), 2303–2322.
Zhang, L., Singh, V.P., 2014. Trivariate flood frequency analysis using discharge time series with possible different lengths: Cuyahoga river case study. J. Hydrol. Eng. 19 (10), 554–555.
Zhang, Q., Chen, Y.D., Chen, X., Li, J., 2011. Copula-based analysis of hydrological extremes and implications of hydrological behaviors in the Pearl River basin. China. J. Hydrol. Eng. 16 (7), 598–607.
Zhang, Q., Xu, C.Y., Jiang, T., Wu, Y., 2007. Possible influence of ENSO on annual maximum streamflow of the Yangtze River, China. J. Hydrol. 333 (2–4), 265–274.
Zhang, Q., Li, J., Singh, V.P., Xu, C.Y., 2013. Copula-based spatio-temporal patterns of precipitation extremes in China. Int. J. Climatol. 33 (5), 1140–1152.
Zhang, S., Tao, F., Zhang, Z., 2016. Changes in extreme temperatures and their impacts on rice yields in southern China from 1981 to 2009. Field Crops Res. 189, 43–50.
Zhao, J., Yan, X., Guo, J., Jia, G., 2012. Evaluating spatial-temporal dynamics of net primary productivity of different forest types in northeastern China based on improved FORCCHN. PLoS One 7 (11), e48131.
Zhao, J., Guo, J., Mu, J., 2015. Exploring the relationships between climatic variables and climate-induced yield of spring maize in Northeast China. Agric. Ecosyst. Environ. 207, 79–90.
Zhao, J., Yang, X., Liu, Z., Lv, S., Wang, J., Dai, S., 2016. Variations in the potential climatic suitability distribution patterns and grain yields for spring maize in Northeast China under climate change. Climatic Change 137 (1–2), 29–42.
Zhang, X., Zhao, X., Jiang, Z., Shao, S., 2017. How to achieve the 2030 CO_2 emission-reduction targets for China's industrial sector: Retrospective decomposition and prospective trajectories. Global Environ. Change 44, 83–97.
Zhou, Y., Ren, G., 2011. Change in extreme temperature event frequency over mainland China, 1961–2008. Clim. Res. 50 (2–3), 125–139.